

## Nonequilibrium kinetics of the transformation of liquids into physical gels

José Manuel Olais-Govea,<sup>1,2</sup> Leticia López-Flores,<sup>1,\*</sup> Martín Chávez-Páez,<sup>1</sup> and Magdaleno Medina-Noyola<sup>1</sup><sup>1</sup>*Instituto de Física “Manuel Sandoval Vallarta,” Universidad Autónoma de San Luis Potosí, Álvaro Obregón 64, 78000 San Luis Potosí, SLP, Mexico*<sup>2</sup>*Escuela de Ingeniería y Ciencias, Instituto Tecnológico y de Estudios Superiores de Monterrey, Av. Eugenio Garza Sada 300, 78211 San Luis Potosí, SLP, Mexico*

(Received 23 September 2017; revised manuscript received 27 August 2018; published 2 October 2018)

A major stumbling block for statistical physics and materials science has been the lack of a universal principle that allows us to understand and predict elementary structural, morphological, and dynamical properties of nonequilibrium amorphous states of matter. The recently developed nonequilibrium self-consistent generalized Langevin equation theory, however, has been shown to provide a fundamental tool for the understanding of the most essential features of the transformation of liquids into amorphous solids, such as their aging kinetics or their dependence on the protocol of fabrication. In this work we focus on the predicted kinetics of one of the main fingerprints of the formation of gels by arrested spinodal decomposition of suddenly and deeply quenched simple liquids, namely, the arrest of structural parameters associated with the morphological evolution from the initially uniform fluid, to the dynamically arrested spongelike amorphous material. The comparison of the theoretical predictions (based on a simple specific model system), with simulation and experimental data measured on similar but more complex materials, suggests the universality of the predicted scenario.

DOI: [10.1103/PhysRevE.98.040601](https://doi.org/10.1103/PhysRevE.98.040601)

In spite of its relevance, there seems to be no universal principle that explains how Boltzmann’s postulate  $S = k_B \ln W$  operates for nonequilibrium conditions, such that it predicts, for example, the transformation of liquids into nonequilibrium amorphous solids such as glasses, gels, etc. [1,2], in terms of molecular interactions. For instance, quenching a simple liquid to inside its gas-liquid spinodal region, normally leads to its full phase separation [3–7]. Under some conditions, however, this process may be interrupted when the denser phase solidifies as an amorphous spongelike nonequilibrium bicontinuous structure with statistically well-defined spatial heterogeneities, whose final mean size  $\xi_a$  depends on the density and final temperature of the quench [8–16].

This process, referred to as *arrested* spinodal decomposition, is revealed by the development of a peak at small wave vectors in the nonequilibrium structure factor  $S(k;t) \equiv \langle \delta n(\mathbf{k}, t) \delta n(-\mathbf{k}, t) \rangle$  of many real [8–14] and simulated [9,11,15,16] gel-forming liquids. Its most remarkable kinetic fingerprint is the fact that the position  $k_{\max}(t)$  of this nonequilibrium peak decreases with waiting time  $t$  until the mean size  $\xi(t) = 2\pi/k_{\max}(t)$  of these heterogeneities saturates at the finite “arrested” value  $\xi_a$ .

Most of the previous experimental and simulation reports [8–12,15,16] acknowledge the notable absence of a fundamental predictive theory that explains the universal and the specific features of the evolution of nonequilibrium properties, such as  $S(k;t)$ . It is not clear, for instance [17], how to extend the classical theory of spinodal decomposition [3–7] to include the possibility of dynamic arrest, or how to incorporate the characteristic nonstationarity of spinodal

decomposition in existing theories of glassy behavior [18,19]. Thus, for example, in spite of its impressive predictive power, illustrated by the existence of attractive glasses in systems with short-ranged attractions [20,21], mode-coupling theory remains in essence an equilibrium theory, unable to describe nonstationary processes such as aging.

The present work starts with the assumption that the manner in which Boltzmann’s postulate explains nonequilibrium states is provided by Onsager’s description of irreversible processes and thermal fluctuations, adequately extended to include spatial and temporal nonlocalities, as well as genuine nonequilibrium conditions [22,23]. Its application as a generic theory of irreversible processes in liquids, referred to as the nonequilibrium self-consistent generalized Langevin equation (NE-SCGLE) theory [23–25], seems to provide the long-awaited fundamental framework to understand the phenomenology of structural glasses and gels in terms of their specific molecular constitution. Judging by its predictions [26–28], this nonequilibrium theory represents a major opportunity for progress in the science and engineering of these materials. The main purpose of this short communication is to report that this theory provides, in particular, a vivid description of the *kinetics* of the *structural* transformation of simple liquids into physical gels by arrested spinodal decomposition, *a feature never before achieved by any other theory*. Here we also illustrate the universal nature of the main qualitative features of these predictions, by comparing them with observations in a wide variety of experimental realizations.

Let us start by considering a generic (“Lennard-Jones-like”) monocomponent simple liquid, with pairwise repulsive core, plus weaker longer-ranged attractive interactions. Assume that we subject this system to an *instantaneous isochoric*

\*llopez@ifisica.uaslp.mx

cooling at waiting time  $t = 0$ , from an initial temperature  $T_i$  to a final temperature  $T_f$ . We then let the system relax under isochoric and isothermal conditions and in the absence of applied external fields. As explained in Refs. [23,28], the essence of the NE-SCGLE theory are the time-evolution equations of the mean value  $\bar{n}(\mathbf{r}, t)$  and of the covariance  $\sigma(\mathbf{r}, \mathbf{r} + \mathbf{x}; t)$  of the fluctuations of the local density  $n(\mathbf{r}, t)$  of particles. To zeroth order in the deviation  $\Delta\bar{n}(\mathbf{r}, t) \equiv \bar{n}(\mathbf{r}, t) - \bar{n}$  from uniformity (see the Appendix), the equation for the covariance becomes the time-evolution equation of the nonequilibrium static structure factor  $S(k; t)$ , which for  $t > 0$  reads

$$\frac{\partial S(k; t)}{\partial t} = -2k^2 D_0 b(t) n \mathcal{E}_f(k) [S(k; t) - 1/n \mathcal{E}_f(k)], \quad (1)$$

where  $D_0$  is the short-time self-diffusion coefficient [29,30]. In this equation  $\mathcal{E}_f(k) \equiv \mathcal{E}(k; \bar{n}, T_f)$  is the Fourier transform of the thermodynamic functional derivative  $\mathcal{E}[\mathbf{r}, \mathbf{r}'; n, T] \equiv \{\delta\beta\mu[\mathbf{r}; n, T]/\delta n(\mathbf{r}')\}$ , evaluated at the uniform density and temperature profiles  $n(\mathbf{r}) = n$  and  $T(\mathbf{r}) = T_f$ , which can be written as  $\mathcal{E}[\mathbf{r}, \mathbf{r}'; n, T] = \mathcal{E}(|\mathbf{r} - \mathbf{r}'|; n, T) = \delta(\mathbf{r} - \mathbf{r}')/n - c(|\mathbf{r} - \mathbf{r}'|; n, T)$  or, in Fourier space, as  $\mathcal{E}(k; n, T) = 1/n - c(k; n, T)$ , where  $c(r; n, T)$  is the so-called direct correlation function.

The key ingredient in Eq. (1) is the  $t$ -dependent mobility function  $b(t)$ , which is in reality a *functional* of the nonstationary structure factor  $S(k; t)$ . As explained in Ref. [24], such functional dependence is determined by the set of NE-SCGLE equations [summarized here as Eqs. (SM1)–(SM5) of the Supplemental Material [31], complemented with Eq. (1) itself]. This strongly nonlinear set of equations must be solved self-consistently. As a result, besides the stationary solutions  $\lim_{t \rightarrow \infty} S(k; t) = S^{\text{eq}}(k; n, T_f) \equiv 1/n \mathcal{E}(k; n, T_f)$ , representing ordinary thermodynamic equilibrium states, Eq. (1) also predicts dynamically arrested stationary solutions  $S_a(k)$  when  $\lim_{t \rightarrow \infty} b(t) = 0$ . A systematic presentation of the predictions of this theory and of their correspondence with the widely observed experimental signatures of the glass transition, started in Refs. [25] and [28] with the description of the transformation of equilibrium hard-sphere (and soft-sphere) liquids into “repulsive” glasses.

A far more interesting prediction arises, however, when Eq. (1) is applied to the description of the spinodal decomposition of Lennard-Jones–like simple liquids [27], illustrated here for analytical simplicity with the hard-sphere plus attractive Yukawa (HSAY) model, defined by the pair potential

$$u(r) = \begin{cases} \infty, & r < \sigma; \\ -\epsilon \frac{\exp[-z(r/\sigma - 1)]}{(r/\sigma)}, & r > \sigma. \end{cases} \quad (2)$$

For given  $\sigma$ ,  $\epsilon$ , and  $z$ , the state space of this system is spanned by the dimensionless number density  $[n\sigma^3]$  and temperature  $[k_B T/\epsilon]$ , denoted simply as  $n$  and  $T$  (i.e., we shall use  $\sigma$  as the unit of length, and  $\epsilon/k_B$  as the unit of temperature); we also refer to the hard-sphere volume fraction  $\phi \equiv \pi n/6$ . The dimensionless time  $[D_0 t/\sigma^2]$  will also be denoted simply as  $t$ . The main findings of Ref. [27], which only analyzed the asymptotic *stationary* solutions of Eq. (1), are summarized in Fig. 1.

In contrast, the present work focuses on the detailed kinetics of  $S(k; t)$  provided by the full solution of Eq. (1) for the same model system subjected to instantaneous isochoric

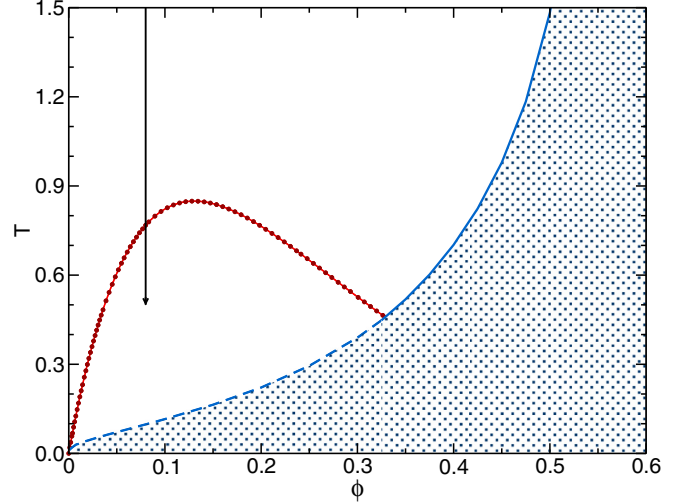


FIG. 1. Nonequilibrium phase diagram of the HSAY ( $z = 2$ ) liquid [27]. At high temperatures and densities, cooling this liquid drives it through the transition (blue solid line) to nonequilibrium repulsive glasses [25]. At intermediate and low densities and temperatures the NE-SCGLE theory predicts that (i) the spinodal line  $T_s(\phi)$  (red dotted line) is a frontier between equilibrium and nonergodic states, (ii) the liquid-glass transition line penetrates inside the spinodal region as a glass-glass transition line (dashed blue line), and (iii) below the composed (solid and dashed) blue line there exists a continuous region of porous repulsive glasses (shaded region). The vertical arrow represents the instantaneous temperature quench referred to in Fig. 2, from an initial high temperature  $T_i = 1.5$ , to a final temperature  $T_f = 0.5$  along the isochore  $\phi = 0.08$ .

quenches illustrated by the vertical arrow in Fig. 1. For this, we adopt a van der Waals (vdW) approximation for the Helmholtz free energy (see Supplemental Material [31] for details), which provides the approximate thermodynamic input  $\mathcal{E}(k; n, T_f)$  needed in Eq. (1). This quench drives the system well inside the spinodal region, where no solution  $S^{\text{eq}}(k; n, T_f)$  exists that corresponds to *spatially uniform* equilibrium states.

Thus, the only possible uniform stationary solution is the nonequilibrium  $S_a(k)$ , and in Fig. 2(a) we present the one corresponding to the quench represented by the arrow in Fig. 1, together with a sequence of snapshots describing the transient  $S(k; t)$ , which starts from the chosen initial value  $S(k; t = 0) = S_i(k) \equiv S^{\text{eq}}(k; \phi, T_i)$  and ends at  $S_a(k)$ . The first feature to notice in the structural kinetics illustrated by these snapshots is the fast but moderate (and rather uneventful) growth of the main peak of  $S(k; t)$  at  $k \approx 2\pi$ , compared with the dramatic development of the nonequilibrium spinodal decomposition peak at smaller wave vectors, whose height  $S_{\text{max}}(t)$  increases, and whose position  $k_{\text{max}}(t)$  decreases, until saturating at the finite values  $S_{\text{max}}^a$  and  $k_a$ , corresponding to  $S_a(k)$  (red dashed line).

This kinetic process is summarized in the insets of Figs. 2(a) and 2(b) by the solid lines, which illustrates the evolution of  $S_{\text{max}}(t)$  and of the wavelength  $\xi(t) = 2\pi/k_{\text{max}}(t)$  associated with  $k_{\text{max}}(t)$ . The other (dashed) lines in both insets correspond to additional processes that differ only in the depth of the quench, i.e., in the final temperature  $T$ . The

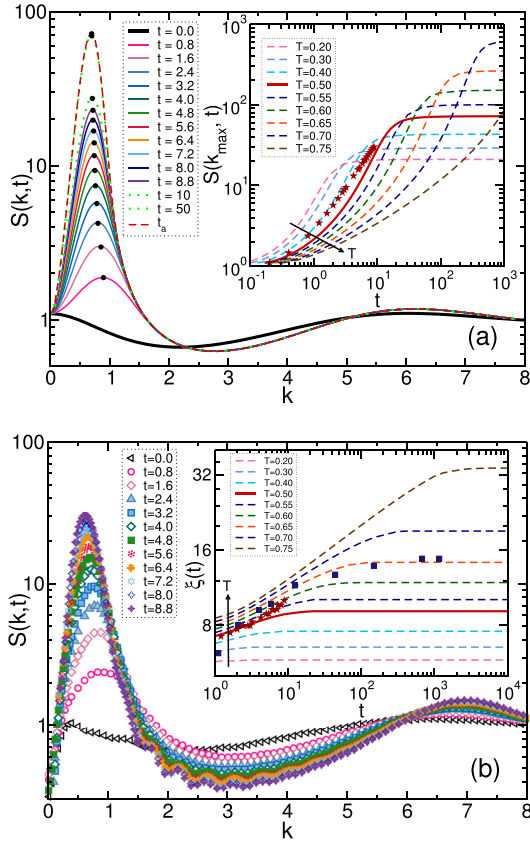


FIG. 2. Snapshots of (a) the theoretical prediction and (b) the Brownian-dynamics simulation results, of the evolution of  $S(k; t)$  from its initial state  $S(k; t = 0)$  toward its asymptotic arrested value  $S_a(k)$  (from bottom to top) for (a) the quench indicated by the arrow in Fig. 1, and (b) for the corresponding simulated quench (see text) at the same waiting times. The dark dots in (a) illustrate the evolution of the height  $S_{\max}(t)$  and position  $k_{\max}(t)$  of the small- $k$  peak of  $S(k; t)$ . The solid line of the insets shows the theoretical evolution (a) of  $S_{\max}(t)$  and (b) of the wavelength  $\xi(t) = 2\pi/k_{\max}(t)$  for this quench, whereas the other lines correspond to similar quenches differing only in the final temperature  $T$  of the quench. The stars are the corresponding results of the simulation in the main panel of (b). The solid squares are experimental results measured in the gelling lysozyme solutions reported in Fig. 2(d) of Ref. [10]. The arrow in the insets indicates increasing temperature  $T$ .

comparison of these illustrative results indicates, for example, that deeper quenches lead to a faster increase (but also earlier arrest) of  $S_{\max}(t)$ . The nonequilibrium evolution of  $\xi(t)$  bears an important morphological and kinetic significance, since it describes the growth and subsequent arrest of the mean size of the spinodal heterogeneities. As illustrated in this inset,  $\xi(t)$  is predicted to increase with waiting time  $t$  and to asymptotically saturate at the finite arrested value  $\xi_a = 2\pi/k_a$ . This maximum size  $\xi_a(T)$  depends on the depth  $T$  of the quench, and as discussed in Ref. [27], it is finite for  $T$  smaller than the spinodal temperature  $T_s$ , but diverges when  $T$  reaches  $T_s$  from below. Thus, although for  $T < T_s$  the emergence of dynamic arrest cancels the possibility of long-time asymptotic divergence of  $\xi(t)$ , before its saturation  $\xi(t)$  appears to follow an apparent algebraic functional form  $\xi(t) \propto t^\alpha$  within a

limited time interval, with an exponent  $\alpha$  that decreases with the depth of the quench, attaining its maximum value when  $T$  approaches  $T_s$ . We have verified that this predicted scenario is qualitatively independent of  $\phi$ , and even of the range  $z^{-1}$  of the attractive term of the pair potential. Furthermore, we also checked its independence on the specific form of the attractive potential, by repeating the same calculations for the hard-sphere plus square-well model liquid (in which the Yukawa tail is substituted by a square well).

To determine to what extent a quantitative comparison can be established with the actual behavior of the HSAY fluid, we performed nonequilibrium Brownian dynamics (BD) simulations on this precise model system to simulate a quench along the isochore  $\phi = 0.1$  from  $T_i = 2.0$  to  $T_f = 0.7$  (see Supplemental Material [31] for details). As it happens, the vdW approximation for  $\mathcal{E}(k; n, T_f)$  locates the critical point (CP) of our system at the state point  $(\phi_c, T_c) = (0.13, 0.85)$ , and not at its actual (simulated) value  $(0.16, 1.22)$ . To scale out these imprecisions, to each simulation state point we assign a theoretical state point  $(\phi, T)$  in a linear proportion as the simulation CP relates to the theoretical CP. Within this correspondence, the simulated quench just defined is analogous to the theoretical quench described in Fig. 2(a). The corresponding simulation results for  $S(k; t)$  are presented in Fig. 2(b).

The comparison between the sequence of simulated snapshots of  $S(k; t)$  with the corresponding theoretical sequence illustrates the qualitative agreement between both descriptions of this nonequilibrium kinetic process. The same comparison also exhibits the quantitative inaccuracies of the approximate theoretical predictions in the early and intermediate stages described by the simulations. Thus, the visual comparison of pairs of snapshots with the same evolution time  $t$ , indicates a slower evolution of the theoretical  $S(k; t)$  compared with the exact evolution represented by the simulations. Also, the position  $k_{\max}(t)$  of the theoretical small wave-vector peak moves more slowly to the left than in the simulations, so that the predicted growth of  $\xi(t)$  is noticeably slower. These features are also illustrated in the insets of Fig. 2.

In spite of this quantitative mismatch between the simulation and the theoretical clocks, we can pair each simulated snapshot with the theoretical snapshot having the same height  $S_{\max}(t)$  (but, obviously, different evolution time  $t$ ). As illustrated in the Supplemental Material [31], this strongly emphasizes the remarkable qualitative similarity between both sequences of snapshots of  $S(k; t)$ . Let us mention that we observed essentially the same semiquantitative agreement when comparing our theoretical predictions for the HSAY model with  $z = 2$  with the BD simulation results for the actual Lennard-Jones system by Lodge and Heyes [15], thus verifying that the main qualitative features of these nonequilibrium structural and morphological processes are independent of the details of the interaction potential.

This prompted us to investigate the extent to which the main qualitative features of this scenario can be recognized in experimental observations where the kinetics of  $S(k; t)$  during the arrested spinodal decomposition of colloidal systems with attractive interactions had been recorded. The result is a general qualitative agreement between the predicted scenario and the experimental observations. This is illustrated already

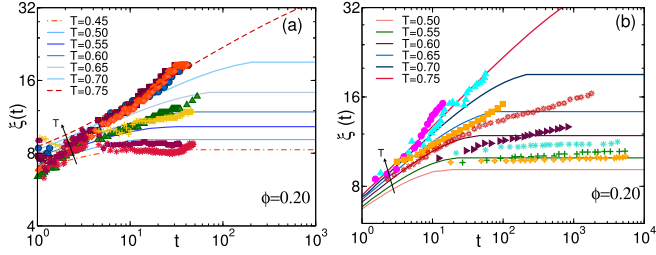


FIG. 3. (a) Theoretical evolution (lines) of the size  $\xi(t)$  for a sequence of quenches for several final temperatures. The symbols are the experimental result measured in the gelling BSA solutions reported in Fig. 7 of Ref. [13], scaled by arbitrary factors to illustrate their qualitative similarity with the predicted theoretical scenario. (b) Same as (a), but here the experimental results correspond to the measurements in the gelling colloid-polymer mixture with colloid-to-polymer size ratio  $\approx 2$  reported in Fig. 5(a) of Ref. [14]. The arrow in the figures indicates increasing temperature  $T$ .

in the inset of Fig. 2(a), which demonstrates that one can superimpose the experimental data of the evolution of  $\xi(t)$  of the full gel-forming process of the globular protein lysozyme in solution reported by Gibaud and Schurtenberger [10], on one of the theoretical curves for  $\xi(t)$  for our HSAY model, even though the attractive forces in this experimental system are surely much shorter-ranged than our Yukawa attraction with  $z = 2$ , and in spite of the difference in the volume fraction of the respective isochores (theory  $\phi = 0.08$ ; experiment  $\phi = 0.15$ ). For the details of this and the following semiquantitative comparison, please see the Supplemental Material [31]. In Fig. 3(a) we expand this comparison, now using similar experimental measurements, this time involving a different globular protein [bovine serum albumin (BSA)] in solution, for which the evolution of  $\xi(t)$  was reported by Da Vela *et al.* [13] for a sequence of quench processes with varying quench depths. Here again the qualitative similarity is remarkable.

The range of the attractive interactions between proteins in the previous two examples is much shorter than the HSAY model with  $z = 2$ , but at least both protein solutions can be regarded as truly monodisperse one-component Brownian liquids. The scenario predicted for this model system, however, can also be recognized in systems with still more complex effective attractions, such as in the colloid-polymer mixture studied by Zhang *et al.* [14], in which the colloids attract each other due to polymer-mediated effective depletion forces. This is illustrated in Fig. 3(b), which corresponds to a colloid-polymer mixture with a ratio of the colloid's radius  $\sigma/2$  to the polymer's radius of gyration  $R_g$  of  $\sigma/2R_g \approx z = 2$ , and to a sequence of polymer-concentration quenches at fixed colloid volume fraction  $\phi = 0.2$ . Once again we observe a remarkable qualitative agreement.

A similar agreement is observed in Fig. 4 between the predicted and the experimental evolution of the colloid-colloid structure factor  $S(k; t)$  measured by Lu *et al.* [8] in a colloid-polymer mixture, this time with a larger colloid to polymer size ratio,  $\sigma/2R_g \approx z = 17$ , and along a more dilute isochore,  $\phi = 0.045$  (see Supplemental Material [31] for details). Figure 4(a) directly compares snapshots of the

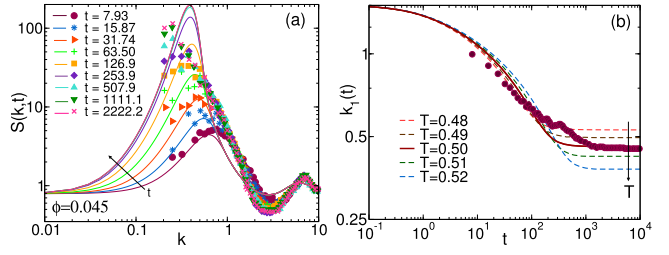


FIG. 4. (a) Snapshots of the theoretical evolution (lines) and of the experimental measurements (symbols) of  $S(k; t)$  in the colloid-polymer mixture reported in Figs. 4(b) and 4(c) of Ref. [8]; the initial and final temperatures of the theoretical quench are  $T_i = 5.0$  and  $T = 0.5$ . (b) Evolution of the first moment  $k_1(t)$  of the experimental (symbols) and theoretical (red solid line)  $S(k; t)$  of the quench in (a); the dashed lines correspond to other final temperatures. The arrow in the figures indicates increasing time  $t$  (a) and temperature  $T$  (b).

structure factor itself and Fig. 4(b) compares the evolution of its first moment,  $k_1(t) \equiv \int_0^{k_c} k S(k; t) dk / \int_0^{k_c} S(k; t) dk$ , where  $k_c$  locates the minimum of  $S(k; t)$  after the low- $k$  peak. The wave vector  $k_1(t)$  bears qualitatively the same morphological information as  $k_{\max}(t)$ . Here, too, the qualitative agreement is quite apparent.

This and the other comparisons discussed above illustrate the experimental fact that the arrest of the growth process severely limits the power-law growth regime and makes it strongly dependent on the depth of the quench. This is in contrast with the universality expected from the perspective of theories that do not consider the emergence of dynamic arrest conditions [5]. Instead, what seems to be universal for the class of systems studied here is the nonequilibrium evolution of the full structure factor and of the main morphological parameter [ $k_{\max}(t)$  or  $k_1(t)$ ] describing the growth and arrest of the spinodal decomposition heterogeneities, the main feature captured by our theory. Let us emphasize, however, that the solution of the NE-SCGLE equations renders much more detailed information on the spatiotemporal nonequilibrium evolution of the structure and dynamics of arresting systems, than those specific features in which we have focused in this Rapid Communication. Other highly remarkable and counterintuitive kinetic features are concomitant to the previously discussed growth and arrest of the spinodal heterogeneities. Their adequate discussion, however, deserves more detailed reports that will be communicated separately.

The authors acknowledge Dr. Fajun Zhang and Stefano da Vela for kindly providing the experimental data of Fig. 3(a) and Professor David A. Weitz and Dr. Peter Lu for kindly providing the experimental data of Figs. 4(a) and 4(b). This work was supported by the Consejo Nacional de Ciencia y Tecnología (CONACYT, México), through Grants No. 242364, No. FC-2015-2-1155, and No. LANIMFE-294155.

#### APPENDIX: THE MAIN APPROXIMATIONS OF THE NE-SCGLE THEORY

According to Ref. [23], the fundamental NE-SCGLE equations are the time-evolution equations of the mean value,

$\bar{n}(\mathbf{r}, t)$ ,

$$\frac{\partial \bar{n}(\mathbf{r}, t)}{\partial t} = D_0 \nabla \cdot b(\mathbf{r}, t) \bar{n}(\mathbf{r}, t) \nabla \beta \mu[\mathbf{r}; \bar{n}(t)], \quad (\text{A1})$$

and of the Fourier transform (FT)  $\sigma(k; \mathbf{r}, t)$  of the covariance  $\sigma(\mathbf{r}, \mathbf{r} + \mathbf{x}; t)$ ,

$$\begin{aligned} \frac{\partial \sigma(k; \mathbf{r}, t)}{\partial t} = & -2k^2 D_0 \bar{n}(\mathbf{r}, t) b(\mathbf{r}, t) \mathcal{E}[k; \bar{n}(\mathbf{r}, t)] \sigma(k; \mathbf{r}, t) \\ & + 2k^2 D_0 \bar{n}(\mathbf{r}, t) b(\mathbf{r}, t), \end{aligned} \quad (\text{A2})$$

of the fluctuations of the local density  $n(\mathbf{r}, t)$  of particles, where  $D_0$  is the particles' short-time self-diffusion coefficient and  $b(\mathbf{r}, t)$  their local reduced mobility. The main external input of these equations is the Helmholtz free energy density-functional  $\mathcal{F}[n, T]$ , or, more precisely, its first and second functional derivatives: the chemical potential  $\mu[\mathbf{r}; n, T] \equiv [\delta \mathcal{F}[n, T] / \delta n(\mathbf{r}')] ]$  and the thermodynamic function  $\mathcal{E}[\mathbf{r}, \mathbf{r}'; n, T] \equiv [\delta \beta \mu[\mathbf{r}; n, T] / \delta n(\mathbf{r}')] ]$ . In Eq. (A2),  $\mathcal{E}[k; \bar{n}(\mathbf{r}, t)]$  is the FT of  $\mathcal{E}[\mathbf{r}, \mathbf{r} + \mathbf{x}; n] \equiv [\delta \beta \mu[\mathbf{r}; n] / \delta n(\mathbf{r} + \mathbf{x})]_{n=\bar{n}(\mathbf{r}, t)}$ .

In principle, these two equations describe the *isochoric* nonequilibrium morphological and structural evolution of a simple liquid of  $N$  particles in a volume  $V$  after being *instantaneously* quenched at time  $t = 0$  to a final temperature  $T_f$ , in the absence of applied external fields. This description, cast in terms of the one- and two-particle distribution functions  $\bar{n}(\mathbf{r}, t)$  and  $\sigma(k; \mathbf{r}, t)$ , involves the local mobility  $b(\mathbf{r}, t)$ , which is in reality a *functional* of  $\bar{n}(\mathbf{r}, t)$  and  $\sigma(k; \mathbf{r}, t)$ , and this introduces strong nonlinearities.

To appreciate the essential physics, however, the best is to provide explicit examples. To do this at the lowest mathematical and numerical cost, let us write  $\bar{n}(\mathbf{r}, t)$  as the sum of its bulk value  $n \equiv N/V$  plus the deviations  $\Delta \bar{n}(\mathbf{r}, t) \equiv \bar{n}(\mathbf{r}, t) - n$  from homogeneity, and in a zeroth-order approximation let us neglect  $\Delta \bar{n}(\mathbf{r}, t)$ . This approximation converts  $\sigma(k; \mathbf{r}, t)$  and  $b(\mathbf{r}, t)$  in the spatially uniform functions  $\sigma(k; t)$  and  $b(t)$ , thus allowing us to write the covariance in terms of the nonequilibrium structure factor  $S(k; t)$  as  $\sigma(k; \mathbf{r}, t) = n S(k; t)$ . As a result, the previous Eq. (A2) becomes Eq. (1) of the Rapid Communication.

- 
- [1] C. A. Angell, K. L. Ngai, G. B. McKenna, P. F. McMillan, and S. F. Martin, *J. Appl. Phys.* **88**, 3113 (2000).
- [2] E. Zaccarelli, *J. Phys.: Condens. Matter* **19**, 323101 (2007).
- [3] J. W. Cahn and J. E. Hilliard, *J. Chem. Phys.* **31**, 688 (1959).
- [4] H. E. Cook, *Acta Metall.* **18**, 297 (1970).
- [5] H. Furukawa, *Adv. Phys.* **34**, 703 (1985).
- [6] J. S. Langer, M. Baron, and H. D. Miller, *Phys. Rev. A* **11**, 1417 (1975).
- [7] J. K. G. Dhont, *J. Chem. Phys.* **105**, 5112 (1996).
- [8] P. J. Lu, E. Zaccarelli, F. Ciulla, A. B. Schofield, F. Sciortino, and D. Weitz, *Nature (London)* **453**, 499 (2008).
- [9] E. Sanz, M. E. Leunissen, A. Fortini, A. van Blaaderen, and M. Dijkstra, *J. Phys. Chem. B* **112**, 10861 (2008).
- [10] T. Gibaud and P. Schurtenberger, *J. Phys.: Condens. Matter* **21**, 322201 (2009).
- [11] L. Di Michele, D. Fiocco, F. Varrato, S. Sastry, E. Eisera, and G. Foffi, *Soft Matter* **10**, 3633 (2014).
- [12] Y. Gao, J. Kim, and M. E. Helgeson, *Soft Matter* **11**, 6360 (2015).
- [13] S. Da Vela, M. K. Braun, A. Dörr, A. Greco, J. Möller, Z. Fu, F. Zhang, and F. Schreiber, *Soft Matter* **12**, 9334 (2016).
- [14] I. Zhang, C. P. Royall, M. A. Faersd, and P. Bartlett, *Soft Matter* **9**, 2076 (2013).
- [15] J. F. M. Lodge and D. M. Heyes, *J. Chem. Soc., Faraday Trans.* **93**, 437 (1997).
- [16] V. Testard, L. Berthier, and W. Kob, *J. Chem. Phys.* **140**, 164502 (2014).
- [17] L. Berthier and G. Biroli, *Rev. Mod. Phys.* **83**, 587 (2011).
- [18] W. Götze, *Complex Dynamics of Glass-Forming Liquids: A Mode-Coupling Theory* (Oxford University Press, New York, 2009).
- [19] J. Langer, *Rep. Prog. Phys.* **77**, 042501 (2014).
- [20] J. Bergenholtz and M. Fuchs, *Phys. Rev. E* **59**, 5706 (1999).
- [21] G. Foffi, G. D. McCullagh, A. Lawlor, E. Zaccarelli, K. A. Dawson, F. Sciortino, P. Tartaglia, D. Pini, and G. Stell, *Phys. Rev. E* **65**, 031407 (2002).
- [22] P. E. Ramírez-González and M. Medina-Noyola, *J. Phys.: Condens. Matter* **21**, 504103 (2009).
- [23] P. E. Ramírez-González and M. Medina-Noyola, *Phys. Rev. E* **82**, 061503 (2010).
- [24] P. E. Ramírez-González and M. Medina-Noyola, *Phys. Rev. E* **82**, 061504 (2010).
- [25] L. E. Sánchez-Díaz, P. Ramírez-González, and M. Medina-Noyola, *Phys. Rev. E* **87**, 052306 (2013).
- [26] L. E. Sánchez-Díaz, E. Lázaro-Lázaro, J. M. Olais-Govea, and M. Medina-Noyola, *J. Chem Phys.* **140**, 234501 (2014).
- [27] J. M. Olais-Govea, L. López-Flores, and M. Medina-Noyola, *J. Chem Phys.* **143**, 174505 (2015).
- [28] P. Mendoza-Méndez, E. Lázaro-Lázaro, L. E. Sánchez-Díaz, P. E. Ramírez-González, G. Pérez-Ángel, and M. Medina-Noyola, *Phys. Rev. E* **96**, 022608 (2017).
- [29] For a colloidal liquid  $D_0$  is the short-time self-diffusion coefficient, while for an atomic liquid  $D_0$  would be given by Eq. (1) of Ref. [30].
- [30] L. López-Flores, P. Mendoza-Méndez, L. E. Sánchez-Díaz, L. L. Yeomans-Reyna, A. Vizcarra-Rendón, G. Pérez-Ángel, M. Chávez-Páez, and M. Medina-Noyola, *Europhys. Lett.* **99**, 46001 (2012).
- [31] See Supplemental Material at <http://link.aps.org/supplemental/10.1103/PhysRevE.98.040601> for details about the theory, experiment, and simulations.